NASA/TP-2003-212158

Analysis of a Radiation Model of the Shuttle Space Suit

Brooke M. Anderson
Swales Aerospace, Hampton, Virginia

John E. Nealy
Old Dominion University, Hampton, Virginia

Myung-Hee Kim
College of William and Mary, Williamsburg, Virginia

Garry D. Qualls and John W. Wilson
Langley Research Center, Hampton, Virginia

March 2003

The NASA STI Program Office . . . in Profile

Since its founding, NASA has been dedicated to the advancement of aeronautics and space science. The NASA Scientific and Technical Information (STI) Program Office plays a key part in helping NASA maintain this important role.

The NASA STI Program Office is operated by Langley Research Center, the lead center for NASA's scientific and technical information. The NASA STI Program Office provides access to the NASA STI Database, the largest collection of aeronautical and space science STI in the world. The Program Office is also NASA's institutional mechanism for disseminating the results of its research and development activities. These results are published by NASA in the NASA STI Report Series, which includes the following report types:

- TECHNICAL PUBLICATION. Reports of completed research or a major significant phase of research that present the results of NASA programs and include extensive data or theoretical analysis. Includes compilations of significant scientific and technical data and information deemed to be of continuing reference value. NASA counterpart of peer-reviewed formal professional papers, but having less stringent limitations on manuscript length and extent of graphic presentations.

- TECHNICAL MEMORANDUM. Scientific and technical findings that are preliminary or of specialized interest, e.g., quick release reports, working papers, and bibliographies that contain minimal annotation. Does not contain extensive analysis.

- CONTRACTOR REPORT. Scientific and technical findings by NASA-sponsored contractors and grantees.

- CONFERENCE PUBLICATION. Collected papers from scientific and technical conferences, symposia, seminars, or other meetings sponsored or co-sponsored by NASA.

- SPECIAL PUBLICATION. Scientific, technical, or historical information from NASA programs, projects, and missions, often concerned with subjects having substantial public interest.

TECHNICAL TRANSLATION. English-language translations of foreign scientific and technical material pertinent to NASA's mission.

Specialized services that complement the STI Program Office's diverse offerings include creating custom thesauri, building customized databases, organizing and publishing research results . . . even providing videos.

For more information about the NASA STI Program Office, see the following:

- Access the NASA STI Program Home Page at ***http://www.sti.nasa.gov***

- Email your question via the Internet to help@sti.nasa.gov

- Fax your question to the NASA STI Help Desk at (301) 621-0134

- Telephone the NASA STI Help Desk at (301) 621-0390

- Write to:
  NASA STI Help Desk
  NASA Center for AeroSpace Information
  7121 Standard Drive
  Hanover, MD 21076-1320

NASA/TP-2003-212158

Analysis of a Radiation Model of the Shuttle Space Suit

Brooke M. Anderson
Swales Aerospace, Hampton, Virginia

John E. Nealy
Old Dominion University, Hampton, Virginia

Myung-Hee Kim
College of William and Mary, Williamsburg, Virginia

Garry D. Qualls and John W. Wilson
Langley Research Center, Hampton, Virginia

National Aeronautics and
Space Administration

Langley Research Center
Hampton, Virginia 23681-2199

March 2003

Available from:

NASA Center for AeroSpace Information (CASI)
7121 Standard Drive
Hanover, MD 21076-1320
(301) 621-0390

National Technical Information Service (NTIS)
5285 Port Royal Road
Springfield, VA 22161-2171
(703) 605-6000

Nomenclature

amu	atomic mass unit
CAD	computer aided design
CAF	computerized anatomical female
CAM	computerized anatomical male
CCA	communications carrier assembly
CCC	contaminant control cartridge
CSDA	continuous slowing down approximation
D	radiation dose (energy deposition in unit mass of material)
DCM	display and control module
d	differential
E	kinetic energy
EMU	extravehicular mobility unit
EVA	extravehicular activity
EVC	extravehicular communicator
EVVA	extravehicular visor assembly
G	energy dissipation per unit length in material
HUT	hard upper torso
HZE	high charge and energy
HZETRN	high charge and energy transport code
I/O	input/output
IDB	in-suit drink bag
ISS	International Space Station
LCVG	liquid cooling and ventilation garment
LEO	low Earth orbit

LTA	lower torso assembly
PDF	probability density function
PLSS	primary life support system
R	range of electrons in material
S	stopping power (energy deposited per unit distance of travel)
SOP	secondary oxygen pack
SPE	solar particle event
STS	Space Transportation System
TMG	thermal micrometeoroid garment
t	distance traveled by electron in material
W	residual energy
$\boldsymbol{\beta}$	unit vector specifying direction
γ	unit vector parallel to local surface
ζ	photon production in material
η	nondimensional transmission function
θ	latitude coordinate
μ	photon extinction coefficient
μ_e	photon absorption coefficient for ionizing energy deposition
σ	interaction cross section
ϕ	differential flux (particles per unit time increment and unit area for unit energy)
φ	longitude coordinate
$\boldsymbol{\Omega}$	solid angle vector
$\boldsymbol{\Omega}_{\min}$	unit vector parallel to local surface

Subscripts:

at	process for atomic electron interaction
e	property of electron
el	process for elastic nuclear scattering
j,*k*	particle type identifiers
p	property of photon
r	process for reactive nuclear interactions

Summary

The extravehicular activity (EVA) required to assemble the International Space Station (ISS) will take approximately 1500 hours with 400 hours of EVA per year in operations and maintenance. With the Space Station at an inclination of 51.6° the radiation environment is highly variable with solar activity being of great concern. Thus, it is important to study the dose gradients about the body during an EVA to help determine the cancer risk associated with the different environments the ISS will encounter. Two different scenarios are looked at: the first is the quiet geomagnetic periods in low Earth orbit (LEO) and the second is during a large solar particle event in the deep space environment. This study includes a description of how the space suit's computer aided design (CAD) model was developed along with a description of the human model. Also included is a brief description of the transport codes used to determine the total integrated dose at several locations within the body. Finally, the results of the transport codes when applied to the space suit and human model and a brief description of the results are presented.

Introduction

The extravehicular activity (EVA) required to assemble the International Space Station (ISS) will take approximately 1500 hours with 400 hours of EVA per year in operations and maintenance. With the Space Station at an inclination of 51.6° the radiation environment is highly variable with solar activity being of great concern (ref. 1). Even during quiet geomagnetic times the radiation that the body experiences during an EVA is vastly different than when inside the ISS. Thus, it is important to study the dose gradients about the body during an EVA to help determine the cancer risk associated with the different environments the ISS will encounter. In addition, a vigorous deep space exploration program requires many EVAs in completing mission objectives, and the degree of protection provided by the space suit is critical to astronaut health, especially during a large solar particle event. An extensive description of various methodologies regarding radiation exposures and protection for humans in space may be found in NASA CP-3360 (ref. 2).

To analytically determine the dose at a given target point several things need to be modeled. The first is the external environment that includes the radiation fields. This study considers both the trapped radiations (protons and electrons) during quiet geomagnetic periods in low Earth orbit (LEO) and a large solar particle event as an exposure in the deep space environment. The second thing that needs modeling is the type of shielding material provided for the astronaut. For this discussion, the materials are the shuttle space suit and the human tissue surrounding a given target point within the body. For modeling of the human, the computerized anatomical male and computerized anatomical female (CAM and CAF, respectively) data sets are used (refs. 3 and 4). Two space suits are in current use within the ISS program: the U.S. shuttle space suit (ref. 5) and the Russian Orlan-M space suit (refs. 6 and 7). This paper concentrates primarily on the U.S. shuttle suit (or extravehicular mobility unit, EMU); planned future work will incorporate the Orlan-M suit. A description of how the shuttle space suit material is modeled is given in appendix A.

The purpose of this paper is to present the details of how the EMU was modeled and to examine its impact on estimates of astronaut health risks. In this respect, the nonuniform distribution of mass of the space suit provides increased shielding in some directions and for some critical organs. These aspects can be most important in terms of health risks and especially critical to evaluation of potential early radiation effects.

Description of the Shuttle Space Suit

Principal components of the shuttle space suit consist of the hard upper torso (HUT), arm assembly, lower torso assembly (LTA), and the extravehicular gloves. The brief description here is taken largely from reference 2 and the major components are shown in figure 1. The HUT is constructed of fiberglass and covered outside with orthofabric, aluminized Mylar®, and neoprene-coated nylon ripstop. These materials, along with values of nominal areal density (mass density multiplied by nominal thickness), are listed in table 1. Under the pressure suit and against the astronaut's body is the liquid cooling and ventilation garment (LCVG) to provide circulation of cooling water and for pickup of vent flow at the extremities. The LTA and arm assembly consist of orthofabric, aluminized Mylar®, neoprene-coated ripstop, polyester, urethane-coated nylon, and water-filled cooling tubes. Extravehicular gloves are similar except for cooling tubes. The materials and nominal areal densities for these components are listed in table 2.

The primary life support system (PLSS), otherwise known as the backpack, consists of the primary oxygen system, oxygen ventilation system, liquid transport system, water feed circuit, secondary oxygen pack (SOP), EMU radio, display and control module (DCM), caution and warning system, contaminant control cartridge (CCC), EMU electrical system, and EMU battery. A listing of these items, their major material constituents, and their approximate masses are given in table 3. The overall dimensions of the PLSS unit measure approximately $23 \times 25 \times 7$ inches.

Due to the sensitivity of the eyes, numerous visors have been constructed to provide maximum protection; this ensemble is called the extravehicular visor assembly (EVVA). Most of the visors are constructed of polycarbonate or polysulfone. A list of the different visors and the helmet along with their material compositions and areal densities is given in table 4.

In prior calculations (ref. 8), the fabric was modeled as 0.28 g/cm^2 with a basal layer of the skin lying about 1 mm below the surface yielding a maximum dose of about 6 cGy/day from electrons. The current study used a more conservative estimate of the mean fabric thickness of 0.186 g/cm^2 with resultant exposures on the order of 14 cGy/day. A more detailed description of how all suit materials were modeled is given in appendices A and B.

CAD Model of the Shuttle Space Suit

The computer aided design (CAD) model was developed in the commercial CAD software package I-DEAS. This package was chosen because of its inherent modeling features: a solid modeler and a finite element modeler, along with a fully integrated solver, with allowances for material definitions. With both the solid and finite element modeler in the same software package considerable time is saved when modifications are needed. With the material definitions and the solver volumes, moments and center of gravity can be calculated for both the solid model and the finite element model, thus allowing for verification and comparisons between the two.

In 1996, a CAD model of a new space suit concept (Mark III) was developed at Langley Research Center. At that time, the Mark III was being developed to be used both on the ISS and as a possible suit for future human missions to Mars. The effort expended on the modeling of the suit focused on simplicity but with an accurate representation of those components that contribute most to radiation shielding (i.e., the visors and the life support system). Effort was also spent to make sure that solid angles subtended by the modeled elements were compatible with those of the true suit. Since then, the Mark III development has ceased and the current shuttle space suit (EMU) and the Russian Orlan M suit are both in use at the ISS. In August 2000 the CAD model was resurrected for application to the current shuttle

suit; later work is planned for inclusion of the Orlan M suit. The current CAD representation of the space suit assembly is shown in figure 2. Most of the modifications done on the model were in the backpack and in reconforming the model to appear more like the Shuttle EMU. The backpack's modifications consisted of rearranging the warning system, the extravehicular communicator (EVC), and the sublimator, along with moving the secondary oxygen tanks down into the SOP, shortening the primary oxygen tanks, adding electronics to the primary oxygen system, and adding the water tanks. Once the backpack modifications were complete, time was spent working on the suit itself, including redesigning the arms to conform more closely to the shuttle suit arms and ensuring solid angle compatibility.

Once the solid model was completed, a finite element model was applied to each part of the EMU. In this process, time was spent to make sure that all the objects were closed and a volume could be calculated. This was done to ensure that there would be no errors when the ray-tracing code (discussed later) was run. Time was also spent making sure all parts were in the same coordinate system. This allowed later combining of all finite element components into a single finite element representation without having to perform translations or rotations. When the solid model of each component was completed and verified they were then meshed with triangular surfaces to create the finite element model. (See fig. 3 for an illustration of the complete finite element model.) Triangular surfaces were used instead of the more common rectangles to limit the growth of round-off errors when running the ray-tracing code, which is discussed subsequently. Once each part had its associated finite element model, it was exported from I-DEAS as a universal file. Once all the EMU parts were exported they were processed by a translator to create object (.obj) files. A total of 28 object files (each representing the different aspects of the EMU) were then processed by a PERL script to create a single object file of the entire EMU. The combined object file was then sent to the Langley GEOLAB immersive desk to aid in checking for errors (i.e., cracks or openings) in the model. With the aid of this three-dimensional environment it was easy to see small details in the model that the average computer monitor could not provide. It was here that cracks were found between the arms and HUT, the helmet and HUT, and between the LTA and HUT. Once the errors were located the CAD model was corrected accordingly. The improved CAD model was then sent back to the three-dimensional environment and reanalyzed for errors. Very minor openings were found in the LTA and legs area, but it was decided that further corrections were unnecessary because the minuscule solid angles involved were not in close proximity to any designated target points.

Ray Tracing the Shuttle Space Suit

The ray tracing was done using Xradical (ref. 9), a program developed at Langley Research Center. The program processes CAD geometry models, in object format, and calculates the directional thickness distribution about specific target points. The inputs needed for Xradical are: the single object file of the CAD model, the coordinates of the given target point (from one of the ≈150 points of the CAM or CAF), and the direction cosine file defining the direction and the number of rays that will determine the directional thickness. The first sets of runs were executed for data files consisting of 1922 directional rays. The 1922-direction cosine data file was initially chosen because each ray has essentially the same solid angle associated with it and the density of data points is practically uniform over the entire spherical surface. Another directional data file of 968 rays was later used to correspond to the existing CAM and CAF data. These direction cosines are based on a spherical coordinate system and consist of 44 points in longitude, φ, and 22 points in latitude, θ, resulting in relatively greater data density around the top and bottom of the sphere than for the middle. Illustrations of these two spherical representations are shown in figures 4 and 5.

Once the ray tracing was completed, several different methods were used to validate the calculations. One visual method is by utilization of a graphical interface procedure (named XCSPH) developed for use

with the Xradical procedure. This program reads in the thickness file created by Xradical and visually displays the thickness contribution of each CAD model component. It has the capability to plot either calculated radiation shielding distributions or the corresponding calculated directional dose and dose rate distributions using input from other programs. It displays these results via a color scale on the surface of a sphere, as shown in figure 6. It is helpful to imagine this sphere centered on the analysis target point so that the color of a particular point on its surface will represent the amount of shielding between the target point at its center and the external radiation environment. This sphere is able to rotate to allow the user to clearly see how much shielding is surrounding the entire target point. The color spectrum can be mapped linearly or logarithmically. The user is also able to select any one, several, or all of the components from those listed in the thickness output files for display of particular contributions. This allows the user to assess shielding contributions from specific components of the geometry.

Another visualization tool used was developed as a PERL code that combines the CAD model with rays that represent thicknesses intercepted within each material. With the object file of the CAD model and the thickness file as inputs, the code outputs a universal file that may be read back into I-DEAS to visually display the rays within the model. This allows the user to make sure that all components are in the correct coordinate system and that there are no spurious thicknesses. An example of the results generated by this procedure is shown in figure 7.

To numerically validate Xradical two methods were used. The first method is to simulate a single direction cosine ray within the CAD model and physically measure the thickness of each component that the ray intersects. This was done for several different rays with several different target points. Tables 5 and 6 give samples of the results. The second method used was to calculate the volume of each component of the solid model itself. This allows one to see how well the finite element model approximates the CAD solid model. Table 7 shows results of the selected volumetric comparisons. It can be seen from tables 5–7 that the largest errors are in the components that have complicated or curved surfaces (e.g., H_2O tanks). This is because the finite element model represents a curved or complex surface with flat triangles, thus introducing some inaccuracies. The accuracy may always be improved by increasing the number of triangles that represent the surface, but at the cost of computational time and storage.

Environment Model

Two environment models of concern here are the LEO environment of ISS and the deep space environment (beyond the geomagnetic field). Although galactic cosmic rays are part of the overall exposure, the intensity is small over the brief EVA periods and thus they are not discussed in this paper. Only the trapped radiations during quiet geomagnetic periods in LEO and a large solar particle event in deep space are considered. The data used to model the trapped radiation environments were obtained during two epochs for solar cycle 20 (the solar minimum of 1964 and the solar maximum of 1970), and best estimates of magnetic field coordinates were taken from current field models at the time of measurement (refs. 10 and 11). The models utilize the environment maps of AE8 and AP8 (refs. 12 and 13, respectively) with superimposed solar cycle variations related to particle source and loss terms. The 1964 analysis using magnetic field model IGRF-65 (epoch 1964) resulted in particle population maps AP8MIN and AE8MIN for trapped protons and electrons, respectively. The 1970 analysis using magnetic field model United States Coast and Geodetic Survey (epoch 1970) resulted in the particle population maps of AP8MAX and AE8MAX. Figures 8 and 9 show the derived model of the time-dependent fields relative to the September 1991 flight environment of Space Transportation System (STS)-48 at 313 nmi and 57° inclination. The STS-48 spectra during September 1991 are shown for comparison with the base models at solar maximum in figures 10 and 11.

On September 29, 1989, a large solar particle event (SPE) occurred containing an iron-rich spectrum with energies approaching 1 A GeV and an approximate energy power index of 2.5 (ref. 14). This SPE is the largest high-energy event in recent time, and 10 times this event matches the ground level data of the SPE of the largest high-energy event ever observed, which occurred on February 23, 1956. It suggests a 10-scaled event as a worst-case event for a design guide of future deep space missions. To analyze the importance of high charge and energy (HZE) ions to human SPE exposure and for a design guide for future deep space missions, the event-integrated fluences of September 29, 1989, are constructed from the measured data. A model developed by Nymmik (ref. 15) describes the proton spectrum with energy above 30 MeV, while Shea and Smart (ref. 16) developed an exponential distribution of protons below 30 MeV. The fluence spectra of the September 29, 1989, event are shown in figures 12 and 13.

Computational Procedures

The types and energy distributions of particles transmitted through a shield material require the solution to the Boltzmann transport equation with appropriate boundary conditions related to the external space radiation environment. The relevant transport equation (ref. 17) for the flux density $\phi_j(\boldsymbol{x},\boldsymbol{\Omega},E)$ of type j particles moving in direction $\boldsymbol{\Omega}$ with energy E is given as

$$\boldsymbol{\Omega}\cdot\nabla\phi_j(\boldsymbol{x},\boldsymbol{\Omega},E) = \sum \int \sigma_{jk}(\boldsymbol{\Omega},\boldsymbol{\Omega}',E,E')\, \phi_k(\boldsymbol{x},\boldsymbol{\Omega}',E')\, d\boldsymbol{\Omega}'\, dE' - \sigma_j(E)\, \phi_j(\boldsymbol{x},\boldsymbol{\Omega},E) \tag{1}$$

where $\sigma_j(E)$ is the media macroscopic cross section for removal of j particles of energy E and $\sigma_{jk}(\boldsymbol{\Omega},\boldsymbol{\Omega}',E,E')$ are the media macroscopic cross sections for various atomic and nuclear processes adding j particles of energy E in direction $\boldsymbol{\Omega}$ including spontaneous disintegration. In general, there are hundreds of particle fields $\phi_j(\boldsymbol{x},\boldsymbol{\Omega},E)$ with several thousand cross-coupling terms $\sigma_{jk}(\boldsymbol{\Omega},\boldsymbol{\Omega}',E,E')$ through the integral. The total cross section $\sigma_j(E)$ with the medium for each particle type of energy E may be expanded as

$$\sigma_j(E) = \sigma_{j,at}(E) + \sigma_{j,el}(E) + \sigma_{j,r}(E) \tag{2}$$

where the first term refers to collision with atomic electrons, the second term is for elastic nuclear scattering, and the third term describes nuclear reactive processes that are ordered as $1{:}10^{-5}{:}10^{-8}$. This ordering allows flexibility in expanding solutions to the Boltzmann equation as a sequence of physical perturbative approximations. The atomic interactions are treated using energy moments wherein the leading term is the usual continuous slowing down approximation. Special problems arise in the perturbation approach for neutrons for which the nuclear elastic process appears as the first-order perturbation and has been the focus of recent research (ref. 18).

The electrons have negligible nuclear reaction cross sections and are dominated by atomic and elastic processes. The basic electron transport is treated by invoking the continuous slowing down approximation (CSDA), where the usual CSDA range has been modified parametrically to account for shortened path length due to multiple scattering. The practical ranges and corresponding range-energy relations are derived from the parameterizations of Tabata, Ito, and Okabe (ref. 19). For an electron of initial energy E, its residual energy, W—after going distance t in an attenuating medium—may be found by solving the equation

$$R(W) = R(E) - t \tag{3}$$

for W when the practical range $R(W) > 0$. Effects of energy fluctuations are incorporated using the energy dissipation formulation of Kobetich and Katz (refs. 20 and 21) wherein actual energy dissipation, G, is expressed in terms of a transmission function, η, as

$$G = d(\eta W)/dt \tag{4}$$

The parameterizations for R and η have been based on numerous electron beam experiments for energy ranges and material elements applicable to space radiation calculations.

The dose at distance t for electron differential flux ϕ_e may then be expressed in terms of the initial and final energy spectra (ref. 22)

$$D(t) = \int G(E,t)\, \phi_e(E)\, dE = \int S(W)\, \phi_e(W)\, dW \tag{5}$$

where S is stopping power. In conformance with the CSDA, the emerging electron spectrum may then be expressed in terms of the initial spectrum as

$$\phi_e(W) = \phi_e(E)G(E)S(E)/[S(W)]^2 \tag{6}$$

In passing through condensed matter, the decelerating electrons give rise to energetic photons (bremsstrahlung), which also contribute to the total energy deposition. The photon production may be expressed in terms of a differential cross section, $\sigma(W,E')$, which represents a probability that an electron of energy W produces a photon of energy E' in its interaction with an atom of the material. These cross sections are generally complicated functions of W, E', and material composition. They have been extensively tabulated by Seltzer and Berger (ref. 23) for wide energy ranges and most elements of the periodic chart. The effective production cross sections for a given material are determined in the present calculations by appropriate spline interpolations of the Berger-Seltzer tabulations.

The photon source term, ς, at distance x and energy E' may be calculated from the electron spectrum as

$$\varsigma(x,E') = \int_{E'}^{W(x)} \phi_e\, \sigma(W,E')\, dW \tag{7}$$

The photons are also being attenuated in accordance with an extinction coefficient, μ, and the photon differential spectrum, $\phi_p(E')$, at distance t may be found using the transfer equation

$$\phi_p(E') = \int \varsigma(x, E')\, e^{-\mu(t-x)}\, dx \tag{8}$$

and the subsequent energy deposition as

$$D_p(t) = \int \mu_e E'\, \phi_p(E')\, dE' \tag{9}$$

where μ_e is an absorption coefficient for photon energy loss resulting in ionizing energy deposition (generally less than the total extinction coefficient, μ). The present code formulation assumes all photons generated propagate in the direction of electron motion.

This simple procedure is of recent vintage, and validation and benchmarking continue at the present time. Calculations for benchmark comparisons made thus far indicate that accuracy has not been substantially degraded at the expense of computational speed. A comparison calculation was made for the electron fluence spectrum shown in figure 14 appropriate to the STS-63 10-day mission at 213 nmi (392 km) at 51.6° inclination using AE8. In the comparison transport calculations, the electrons are assumed to be normally incident on a semi-infinite water slab. The Monte Carlo code TIGERP (ref. 24) was used to validate the computation with the simplified procedure. The very favorable agreement of the two calculations is evident in figure 15 for the electron and photon doses.

The needed outputs from the transport codes are the dose versus depth characteristics for a given environment. These curves describe the energy deposition as particles penetrating the specified materials. Such attenuation characteristics are exhibited in figures 16 and 17 using transport calculations for the LEO environment of STS-48 interacting with a simulated space suit polyester fabric (48 percent C, 42 percent H, 9 percent O by mass). The electron transport was calculated with the deterministic code just described, while the computed transport of trapped protons was performed using the high charge and energy transport (HZETRN) code (refs. 25 and 26). It is seen that both electron and proton doses can be quite large for small penetration depths; in each case the particles attenuate rather quickly. At moderate depths the calculated exposures have decreased markedly, and at nominal depths space suit areal densities ($\approx$0.2 to 2 g/cm^2) are of comparable magnitudes.

Figures 18 and 19 show the dose versus depth curves in tissue from various components within a spherical shell of space suit fabric material for the September 29, 1989, SPE. The dose is dominated by the proton fluence over most shielding thicknesses. The dose equivalent from helium ions gives an important contribution for thickness regarding the space suit fabric. The heavier ions are always of less importance in the exposure. It is clear from the results in figure 20 that very high skin exposures can be expected for this event. However, even a modest amount of additional shielding of the suit is expected to have important effects in reducing radiation exposures. Some caution in redesign is still warranted because mobility and comfort to the astronaut is a key issue in space operations. As can be seen in the figures, there is a slow but significant decline in dose and dose equivalent with larger shield thickness indicating definite advantage is to be gained by the more massive components of the suit and the self-shielding of critical tissues of the astronaut's body. The primary life support system will provide substantial shielding in these cases. The total dose and dose equivalent due to all heavy ion exposures from the SPE are shown in figure 20.

Optional results from the transport calculations include the energy spectra of transported radiations. Figures 21 and 22 show sample differential electron and photon energy spectra for the electron transport code applied to the modeled EMU fabric for the nominal thickness (0.186 g/cm^2) and twice that thickness. The electrons are strongly attenuated over relatively small distances, whereas the photons are shown to have a slight increase over much of the energy range, indicative of their more penetrating nature.

Examples of Computational Results

To demonstrate typical computational results two CAM body points have been chosen: a skin exposure point on the lower right shin and a point on the right ocular lens. The coordinate system used corresponds to the CAM coordinate system, which is fundamentally a Cartesian right-hand system, with the origin at top of head and vertical distances increasing downward. The positive directions of the x- and y-axes are forward through the chest and the right shoulder, respectively. In the usual spherical coordinate representation (polar angle θ, azimuth φ), the CAM model formulation used in the present analysis

consists of 968 directions (22 polar angles θ and 44 evenly distributed azimuth angles associated with each θ). For the leg point, the space suit material is in close proximity with the skin and is taken as a single layer of mean areal density of 0.186 g/cm^2 (composition 48 percent C, 42 percent H, 9 percent O by mass). For the lens point, the helmet was modeled by a single polysulfone layer (50 percent C, 40.7 percent H, 7.4 percent O, 1.9 percent S). For the sample calculations shown here, EMU thicknesses encountered along rays emanating from the dose target point during the ray tracing were scaled to equivalent thicknesses of these two materials. The associated body tissue thicknesses were also scaled accordingly.

Figures 23–26 illustrate some of the directional characteristics of the exposures obtained from the combined EMU CAD model enclosing the CAM body model. Figures 23 and 24 demonstrate the radial directional doses of exposure from the LEO trapped electrons from the orbit-averaged STS-48 mission on the shin target point. Figures 25 and 26 show the directional dose of the lens point during the September 1989 event while on the lunar surface. The ray patterns in figures 23 and 25 are depicted for the sequence of polar angles in an *x*-*z* plane, with length of rays proportional to directional dose magnitudes. The effects of increasing thickness of penetration for directions away from the normal of the space suit fabric are clearly seen. The entirety of directional dose values about the selected CAM target point is plotted in figure 24. Similar results are given in figure 26 for the right ocular lens within the helmet. The abscissas of the plots for figures 24 and 26 may be considered as quasi—two-dimensional with each polar angle represented by the values calculated for its associated azimuth sweep, hence the cyclic nature of the plotted values. The peak values for each cycle are indicative of the direction in which the target point is nearest the surrounding space suit material. (Note that the increasing azimuth cycle number in the plots shows progression of the polar angle from downward to upward direction, i.e., CAM toe → CAM head.) In figure 26, the sudden drop in cyclic peak values above the horizontal (about cycle 11) is a result of the added attenuation of the LEO electrons by the helmet visors.

It is recognized that the information displayed in figures 18–26 does not represent end-point results of a complete dosimetric calculation, but it is felt that such diagnostic checks are essential in validating the complex procedures involved in making complete analyses that usually require a vast number of essentially repetitive operations. For the two target points discussed herein, the resultant integrated dose values are given in table 8.

In the event of a large geomagnetic storm, the electron fluence has been known to increase up to four orders of magnitude in less than an hour. In this case, the lens and skin dose rates would increase by such a factor (and may be more penetrating due to acceleration processes). It is clear that potentially large exposures can occur and timely shelter in the ISS is required during such periods.

Concluding Remarks

The purpose for the present development of the EMU-CAM configuration coupled with the radiation transport codes was to provide a means for generating accurate and comprehensive exposure evaluations in a time frame that allows a more or less immediate, as opposed to after the fact, application. For example, scenarios with time-varying external environments may be examined quickly; impact of EMU modifications on shielding properties may be assessed and/or optimized. In a specific analysis, the time consumed in input/output (I/O) setup was usually far greater than procedure execution itself, and routine validation diagnostics (usually consisting of optional ancillary calculations) were of paramount importance. Such diagnostic procedures were incorporated in the formulation in order that they may be readily activated when configuration or I/O structures were modified.

All computational elements described here are available for detailed and comprehensive astronaut space radiation exposure evaluations for EVA scenarios. Code validation and streamlining have been performed to the extent that full implementation with the space suit-CAM combination may be carried out for a distribution, or grid, of target points throughout the configuration. As of now, no special effort has been made to assess run time for such an application, but a rough estimate for generating a reasonably complete body exposure dose map (≈150 CAM target points) may be carried out in a matter of minutes in serial calculation on a machine with moderate computational speed. Execution on parallel-processing machines should greatly reduce run times, and plans are in place to provide a source code version that takes advantage of parallel-processor implementation. The calculations using these transport codes provide a means for generating accurate and comprehensive exposure evaluations in a time frame that allows a more or less immediate application. Without the use of Monte-Carlo simulations, the computational time needed to complete an entire grid of CAM points is on the order of a few minutes. This allows models with time-varying external environments to be examined quickly, thus allowing the impact of EMU modifications on shielding properties to be assessed and/or optimized.

As can be seen in table 8, the dose during quiet geomagnetic times for points where only the suit is shielding is considerably higher than in places where there is extra material and/or hardware. Thus it was shown that the space suit fabric (TMG/LCVG) is less effective in protecting the skin from exposure than previously assumed and could be greatly improved. Figures 17 and 20–23 show that only modest additions to the fabric have large payoffs in protection. As for points that are near the visors or the primary life support system, these are well protected and need no extra shielding. For an SPE event, it can be seen that the dose for both the lens and skin is extremely high and that the EMU is in no way adequate to protect the astronaut.

It was clear from the present analysis and results that the space suit has important features that will have some benefit for reducing astronaut health risks under extreme exposure conditions in space. Even so, there was some weakness in the space suit design, which was already clear. Mainly the attention has presently been given to the space suit fabric (TMG/LCVG), which was less effective in protecting the skin from exposure than previously assumed and could be greatly improved. Analysis has begun to include the tubing in the LCVG garment, and a brief description of the tube modeling procedure and results is given in appendix B. This optional subroutine does take additional computational time and its recommended use is for skin points that are thought to obtain high electron doses only.

References

1. Anderson, B. M., et al.: Shuttle Spacesuit Model Development. Paper No. 2001-01-2363 in Proc. 31st International Conference on Environmental Systems (ICES), Orlando, FL, July 9–12, 2001.

2. Wilson, J. W.; Miller, J.; Konradi, A.; and Cucinotta, F. A. (eds.): *Shielding Strategies for Human Space Exploration*. NASA CP-3360, 1997.

3. Billings, M. P.; and Yucker, W. R.: The Computerized Anatomical Man (CAM) Model. Report MDC G4655, McDonnell Douglas Corp., Huntington Beach, CA, Sept. 1990.

4. Yucker, W. R.; and Huston, S. L.: Computerized Anatomical Female—Final Report. Rept. MDC H6107, McDonnell Douglas Corp., Huntington Beach, CA, Sept. 1990.

5. Kozloski, L. D.: U. S. Space Gear: Outfitting the Astronaut. Smithsonian Institution Press, Washington, DC, 1994.

6. Severin, G. I.: Design to Safety: Experience and Plans of the Russian Space Suit Programme. *Acta Astronaut.*, vol. 32, no. 1, 1994, pp. 15–23.

7. Abramov, I. P.: The Experience in Operation and Improving the Orlan-Type Space Suits. *Acta Astronaut.*, vol. 36, no. 1, 1995, pp. 1–12.

8. Wilson, J. W.; Tweed, J.; Zeitlin, C.; Kim, M. Y.; Anderson, B. M.; Cucinotta, F. A.; Ware, J.; and Persans, A. E.: Shuttle Spacesuit: Fabric/LCVG Model Validation. Paper No. 2001-01-2372 in Proc. 31st International Conference on Environmental Systems (ICES), Orlando, FL, July 9–12, 2001.

9. Qualls, G. D.; and Boykin, R.: *Space Radiation Shielding Analysis by CAD Techniques*. NASA CP-3360 (Chap. 17), 1997, pp. 365–382.

10. Atwell, W.; Beever, E. R.; Hardy, A. C.; Richmond, R. G.; and Cash, B. L.: Space Radiation Shielding Analysis and Dosimetry for the Space Shuttle Program. In *High Energy Radiation Background in Space*, A. C. Rester and H. I. Trombka, eds. AIP Conference Proc. No. 186, 1989, pp. 289–296.

11. Wilson, J. W.; Kim, M. Y.; Shinn, J. L.; Tai, H.; Cucinotta, F. A.; Badhwar, G. D.; Badavi, F. F.; and Atwell, W.: *Solar Cycle Variation and Application to the Space Radiation Environment*. NASA/TP-1999-209369, 1999.

12. Vette, J. I.: The AE-8 Trapped Electron Model Environment. NSSDC/WDC-A-R&S 91-24, NASA Goddard Space Center, Nov. 1991.

13. Sawyer, D. M.; and Vette, J. I.: *AP-8 Trapped Proton Environment for Solar Maximum and Solar Minimum*. NASA TM X-72605, 1976.

14. Tylka, A. J.; Dietrich, W. F.; and Bober, P. R.: High-Energy Solar Heavy Ions From IMP-8. Naval Res. Lab. Paper at Workshop on Impact of Solar Energetic Particle Events for Design of Human Missions, Center for Adv. Sp. Studies, Houston, TX, Sept. 9–11, 1997.

15. Nymmik, R.: Probabilistic Model for Fluences and Peak Fluxes of Solar Particles. Moscow State Univ. Paper at Workshop on Impact of Solar Energetic Particle Events for Design of Human Missions, Center for Adv. Sp. Studies, Houston, TX, Sept. 9–11, 1997.

16. Shea, M. A.; and Smart, D. F.: A Summary of Major Solar Proton Events. *Solar Phys.*, vol. 127, June 1990, pp. 297–320.

17. Wilson, J. W.; Townsend, L. W.; Schimmerling, W.; Khandelwal, G. S.; Khan, F.; Nealy, J. E.; Cucinotta, F. A.; Simonsen, L. C.; Shinn, J. L.; and Norbury, J. W.: *Transport Methods and Interactions for Space Radiations*. NASA RP-1257, 1991.

18. Clowdsley, M. S.; Heinbockel, J. H.; Kaneko, H.; Wilson, J. W.; Singleterry, R. C.; and Shinn, J. L.: A Comparison of the Multigroup and Collocation Methods for Solving the Low-Energy Neutron Boltzmann Equation. *Ca. J. Phys.*, vol. 78, 2000, pp. 45–56.

19. Tabata, T.; Ito, R.; and Okabe, S.: Generalized Semiempirical Equations for the Extrapolated Range of Electrons. *Nucl. Inst. & Meth.*, vol. 103, 1972, pp. 85–91.

20. Kobetich, E. J.; and Katz, R.: Energy Deposition by Electron Beams and δ Rays. *Phys. Rev.*, vol. 170, no. 2, June 1968, pp. 391–396.

21. Kobetich, E. J.; and Katz, R.: Electron Energy Dissipation. *Nucl. Inst. & Meth.*, vol. 71, 1969, pp. 226–230.

22. Cucinotta, F. A.; Katz, R.; and Wilson, J. W.: Radial Distribution of Electron Spectra for High-Energy Ions. *Radiat. Environ. Biophys.*, vol. 37, 1998, pp. 259–265.

23. Seltzer, S. M.; and Berger, M. J.: Bremsstrahlung Spectra From Electron Interactions With Screened Atomic Nuclei and Orbital Electrons. *Nucl. Inst. & Meth. Phys. Res.*, vol. B12, pp. 95-134, 1985.

24. Halbleib, J. A.; Kensek, R. P.; Mehlhorn, T. A.; Valdez, G. D.; Seltzer, S. M.; and Berger, M. J.: ITS Version 3.0: The Integrated TIGER Series of Coupled Electron/Photon Monte Carlo Transport Codes. SAND 91-1634, Sandia National Lab., Mar. 1992.

25. Wilson, J. W.; Badavi, F. F.; Cucinotta, F. A.; Shinn, J. L.; Badhwar, G. D.; Silberberg, R.; Tsao, C. H.; Townsend, L. W.; and Tripathi, R. K.: *HZETRN: Description of a Free-Space Ion and Nucleon Transport and Shielding Computer Program*. NASA TP-3495, 1995.

26. Kim, M. Y.; Wilson, J. W.; Cucinotta, F. A.; Simonsen, L. C.; Atwell, W.; Badavi, F. F.; and Miller, J.: *Contribution of High Charge and Energy (HZE) Ions During Solar-Particle Event of September 29, 1989*. NASA/TP-1999-209320.

Table 1. Components of Hard Upper Torso (HUT)

Layer	Material	Areal density, g/cm^2
Outer layer	Orthofabric-Teflon/Nomex/Kevlar®	0.049
Insulation	Aluminized Mylar®–5 plies	0.014
Inner layer	Neoprene-coated nylon ripstop	0.028
Hard shell	Fiberglass	0.354
LCVG	Spandex/water/ethylvinylacetate	0.154

Table 2. Constituents of Space Suit Fabric With Water Tubes

Material	Areal density, g/cm^2
Orthofabric-Teflon/Nomex/Kevlar®	0.049
Reinforced aluminized Mylar®	0.014
Neoprene-coated ripstop	0.028
Dacron polyester	0.021
Urethane-coated nylon	0.014
Nylon/Spandex/water/ethylvinylacetate	0.154

Table 3. Major Material Constituents and Approximate Masses of PLSS

Subsystem	Component	Material constituent	Mass, kg
O_2 ventilating circuit	Regulators, vessels, fans	Fe, Cr, Ni, Cu, …	14.4
	LiOH assembly	LiOH, Fe	6.4
H_2O transport	Pump, valves, sensors	Fe, Cu	6.5
	Liquid	H_2O	4.5
Electrical system	Electronics	Si, O, Cu, …	15.1
	Battery	ZnAgO	4.5
O_2 purge system	Bottles	Fe, O_2	8.6
	Regulator	Fe	4.2

Table 4. Shuttle Space Suit Helmet and EVVA Constituents

Component	Material	Areal density, g/cm^2
Outer layer	Orthofabric-Teflon/Nomex/Kevlar®	0.049
Insulation	Aluminized Mylar®–5 plies	0.014
Spacer	Dacron fiber–5 plies	0.011
Inner liner	Teflon	0.028
EVVA shell	Polycarbonate	0.381
Sun visor	Polysulfone	0.190
Eyeshade	Polysulfone	0.190
Protective visor	Polycarbonate	0.182
Helmet	Polycarbonate	0.182

Table 5. Comparison of CAD Model to Ray-Tracing Results for Skin Point #36

Ray no. 236	Thickness file, g/cm^2	CAD model, g/cm^2	Error, percent
HUT	0.6572	0.6349552	3.5
Right leg	1.63	1.624429	0.22
Left leg	1.97	1.955015	0.51

Table 6. Comparison of the CAD Model to Ray-Tracing Results for Skin Point #36

Ray no. 755	Thickness file, g/cm^2	CAD model, g/cm^2	Error, percent
Backpack cover	0.5199	0.5199595	0.01
EVC	13.31	13.30605	0.03
Backpack cover	2.389	2.388342	0.03
LTA	2.878	3.133541	8.1

Table 7. Comparison of Finite Element Model and CAD Solid Model Volumes

Component	Solid model volume, cm^3	Finite element volume, cm^3	Error, percent
Backpack cover	7568.2	7570	0.2378
Contaminant control	2760	2760	0
H_2O storage	6844.62	6971	1.846
H_2O tanks	375.462	360.9	3.878
Warning system	2280	2280	0
Center eyeshade	364.218	356	2.256
EVVA shell	1244.71	1235	0.78
Head rest	99.2783	98.76	0.522
HUT	2393.34	2391	0.097
Battery	1200	1200	0

Table 8. Total Integrated Doses for Lens and Shin Target Points

Radiation source	Lens dose, cGy	Leg skin dose, cGy
Trapped electrons	0.026	1.69
Bremsstrahlung	0.0014	0.0032
September 1989 SPE (lunar surface)	82.7	412

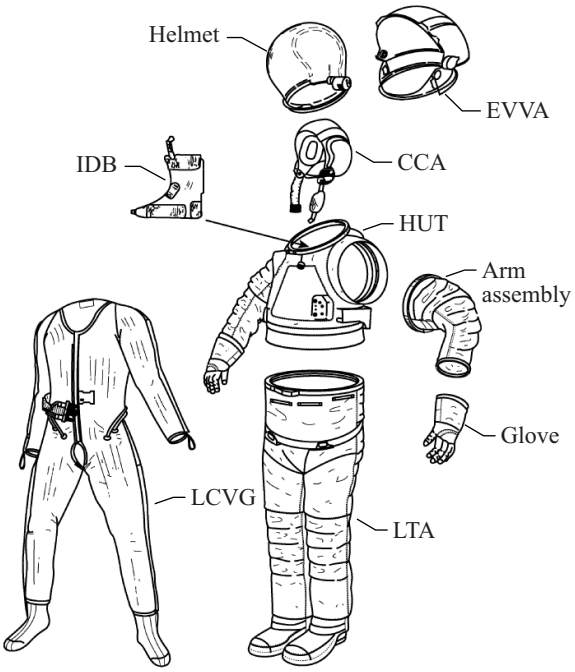

Figure 1. Basic components of shuttle space suit.

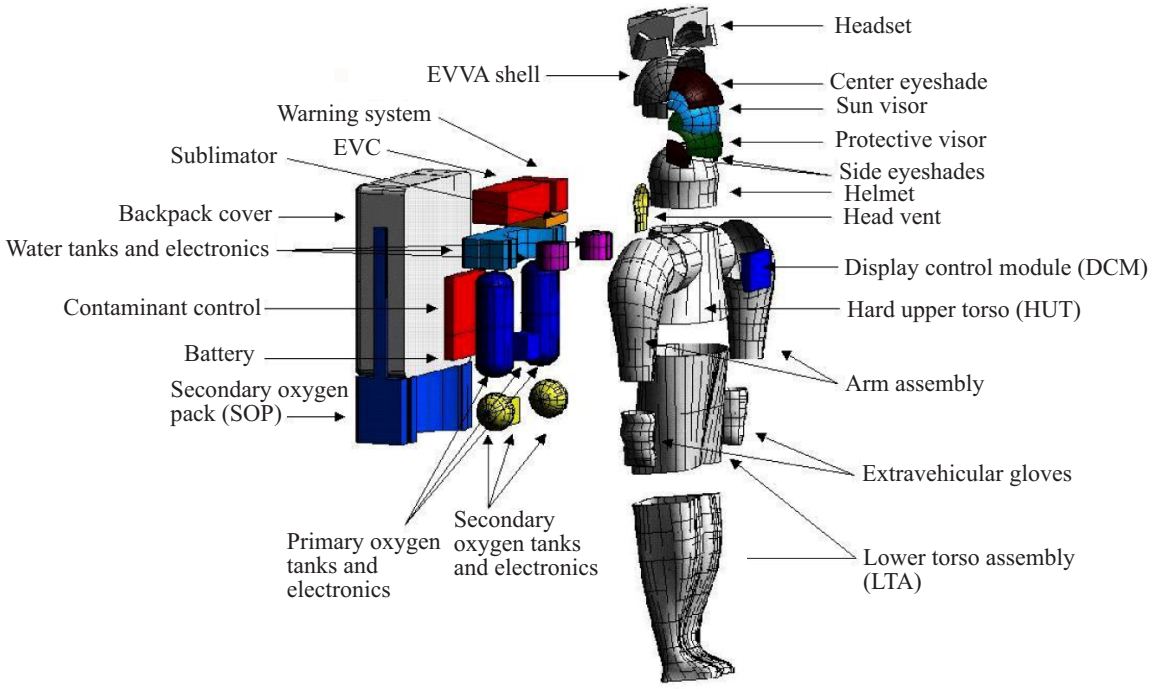

Figure 2. CAD model of shuttle space suit.

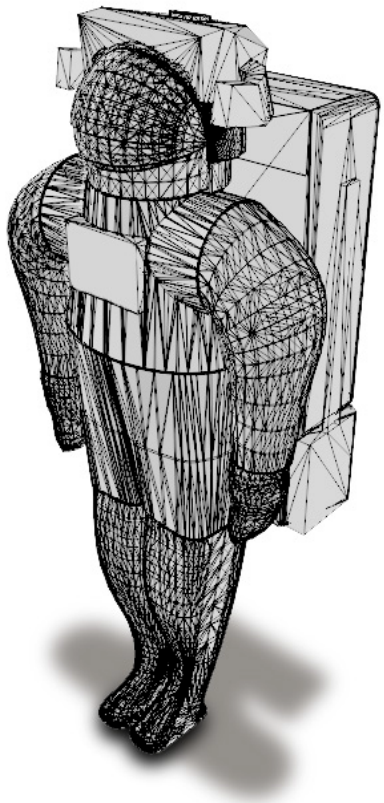

Figure 3. Finite element model of EMU.

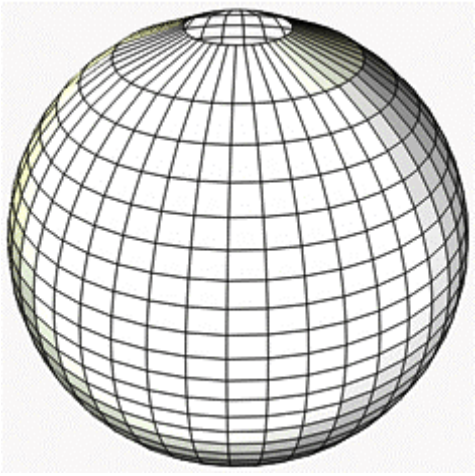

Figure 4. Sphere representing 968 directional cosine input file.

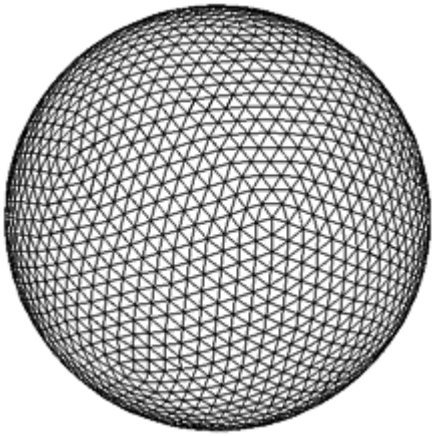

Figure 5. Sphere representing 1922 directional cosine input.

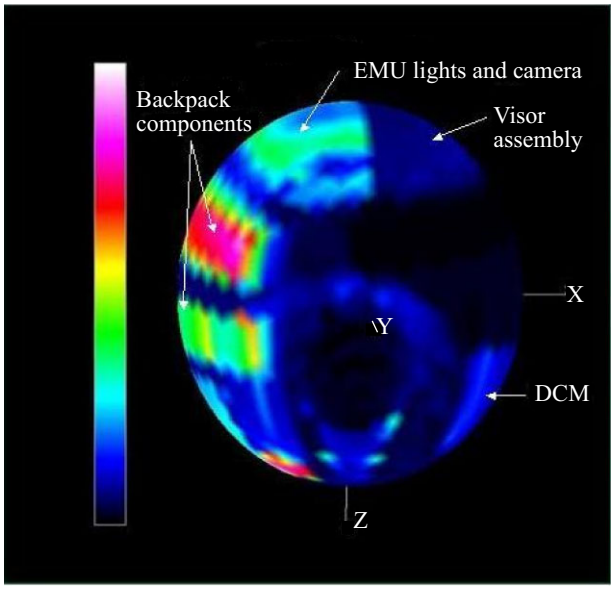

Figure 6. Visualization of space suit shield materials distribution of point in sternum.

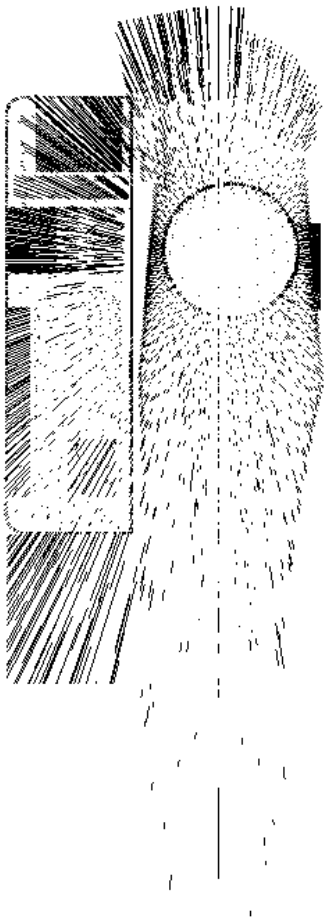

Figure 7. Projected space suit material crossings along 1922 ray directions.

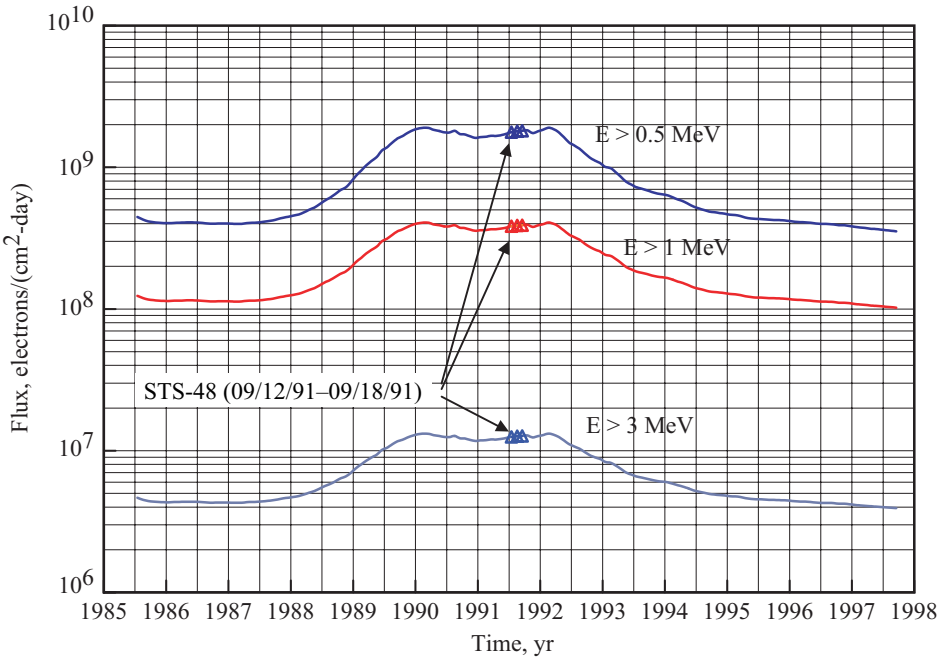

Figure 8. STS-48 electron environment.

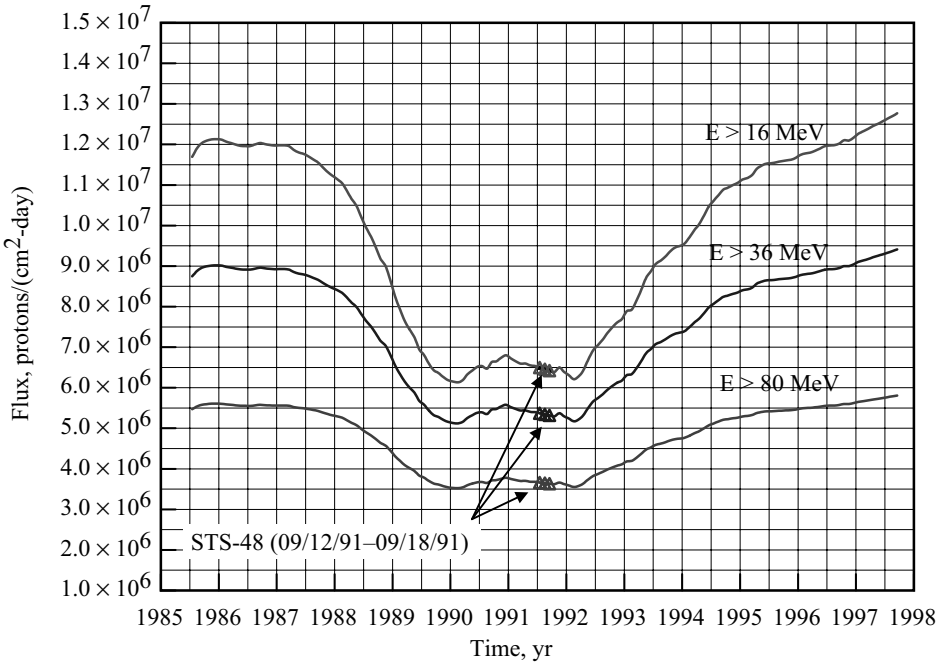

Figure 9. STS-48 proton environment.

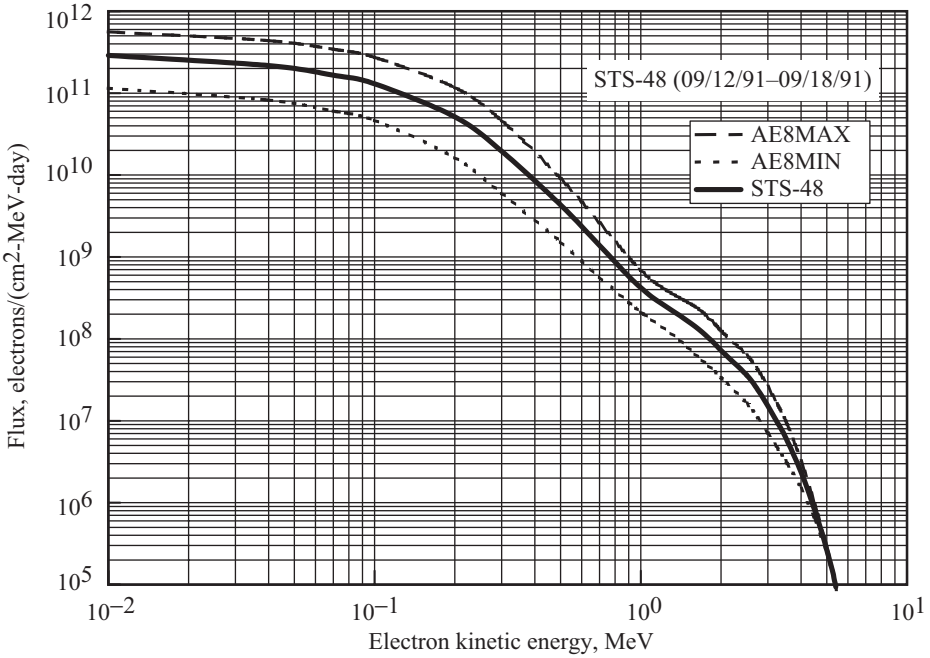

Figure 10. STS-48 electron environment and AE8 model.

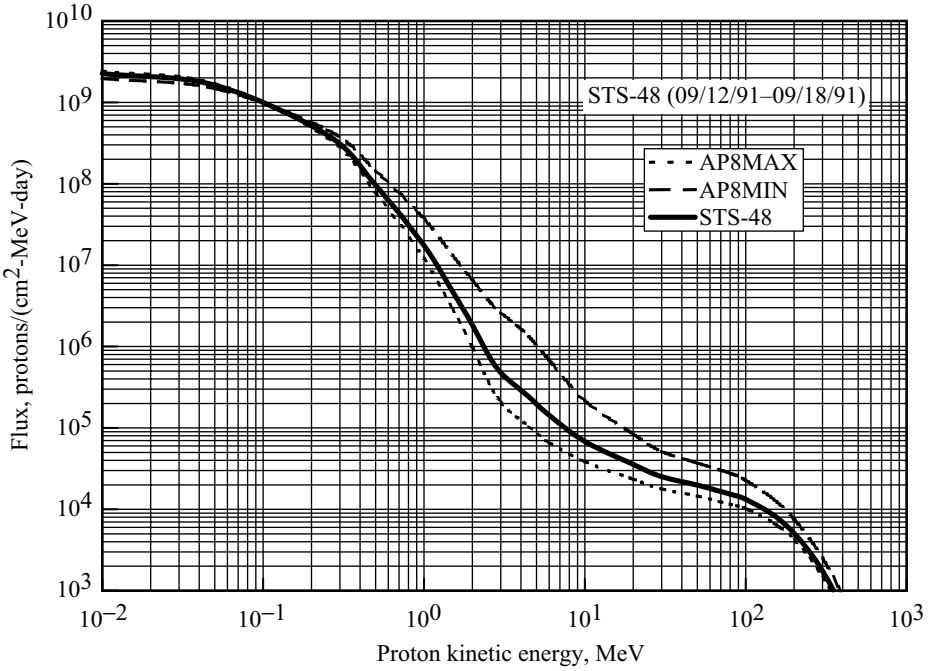

Figure 11. STS-48 proton environment and AP8 model.

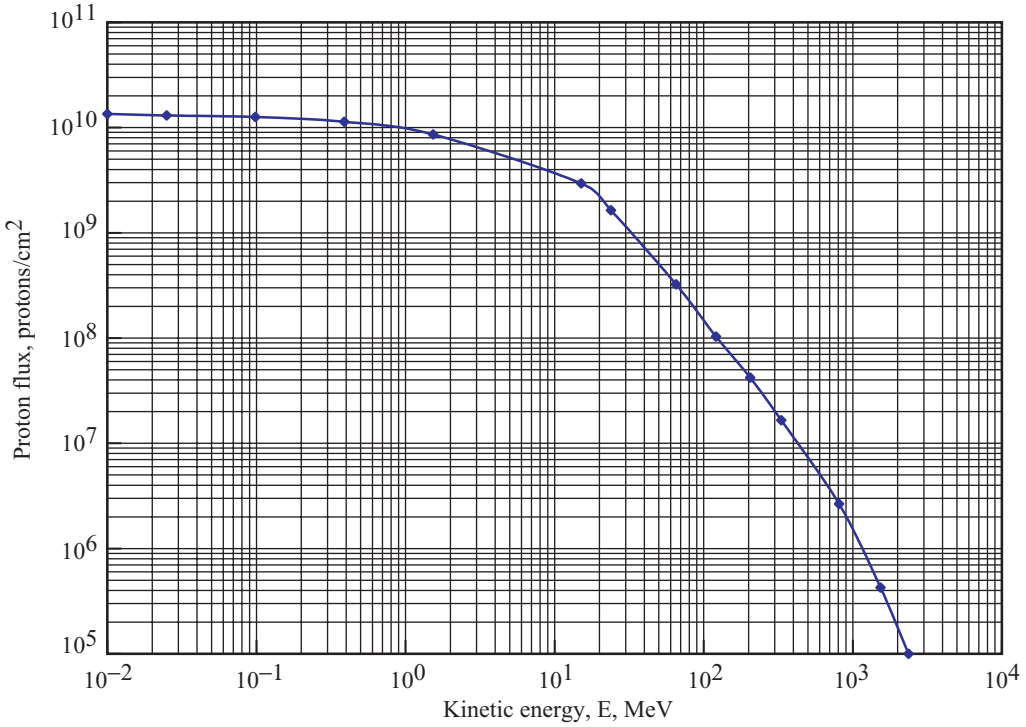

Figure 12. September 29, 1989, solar proton spectrum.

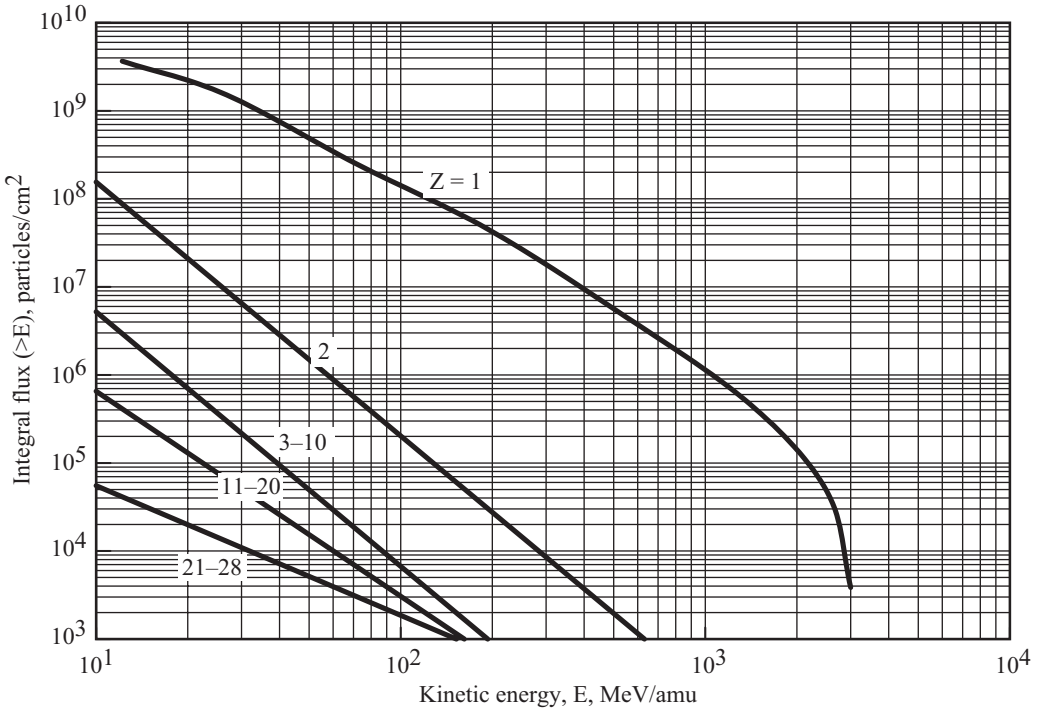

Figure 13. September 29, 1989, solar heavy ion spectra.

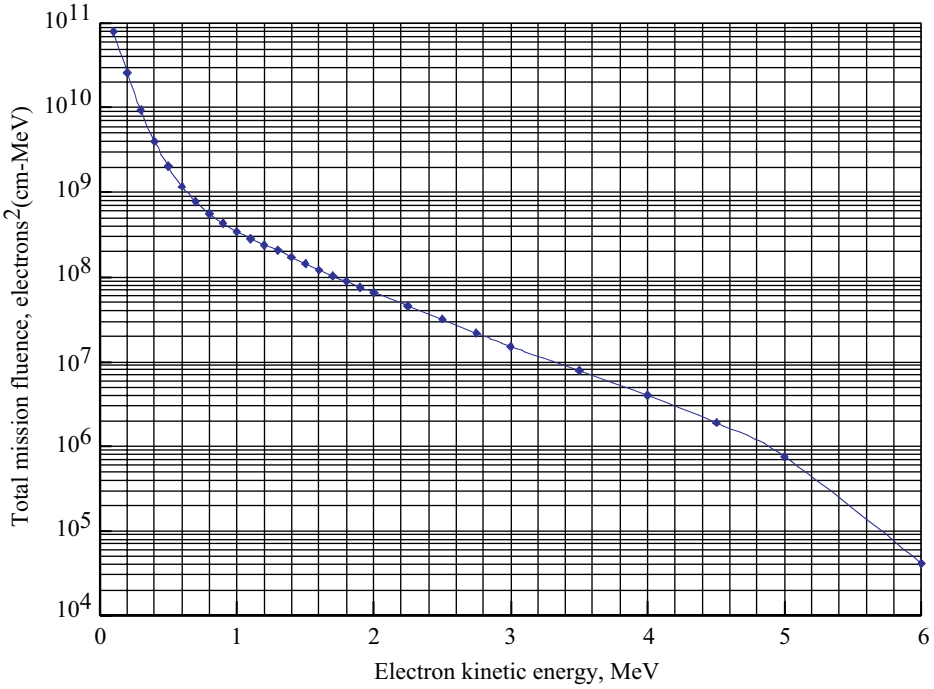

Figure 14. Electron fluence for 10-day mission of STS-63.

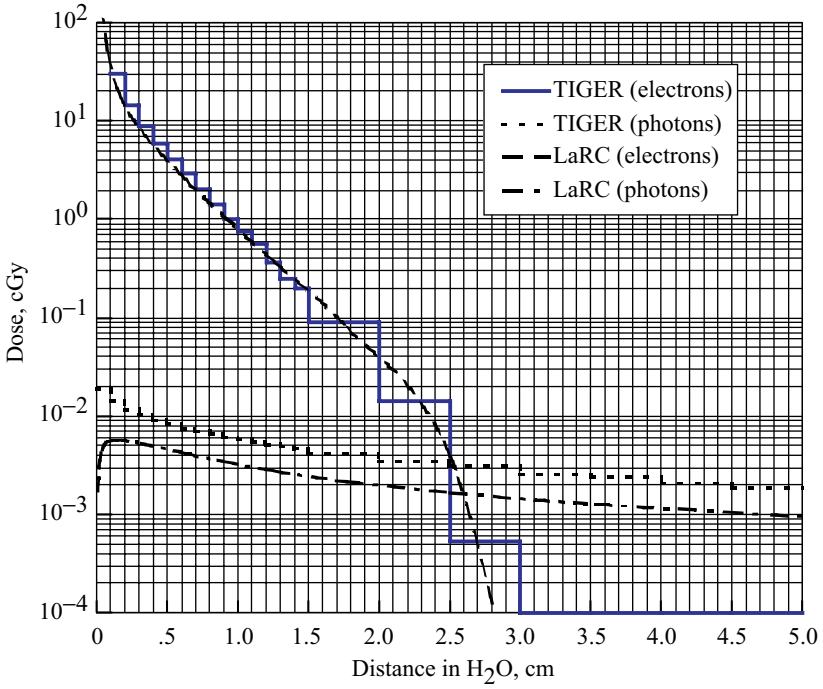

Figure 15. Dose versus depth in H_2O for electron spectrum of mission STS-63.

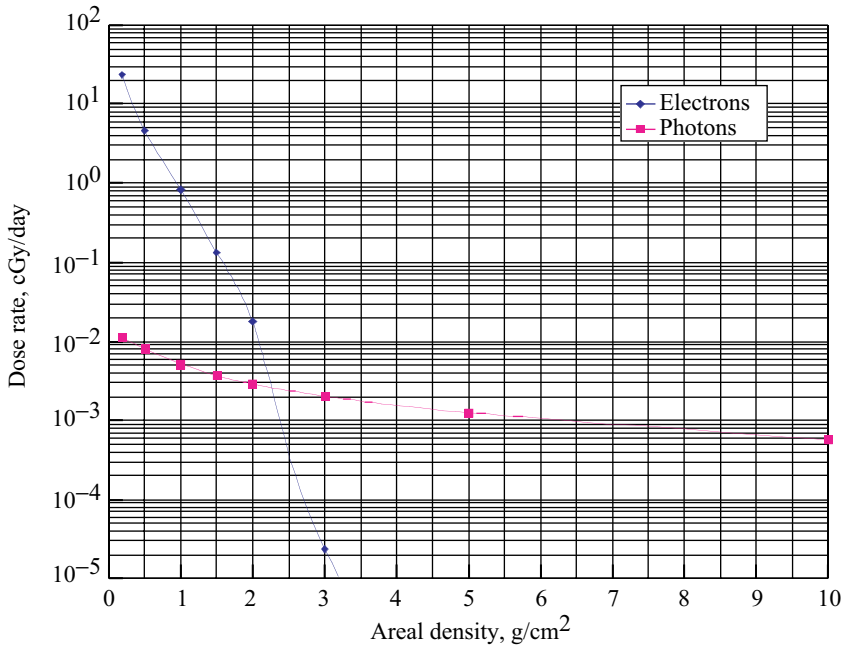

Figure 16. Dose versus depth in space suit fabric for STS-48 electron spectrum.

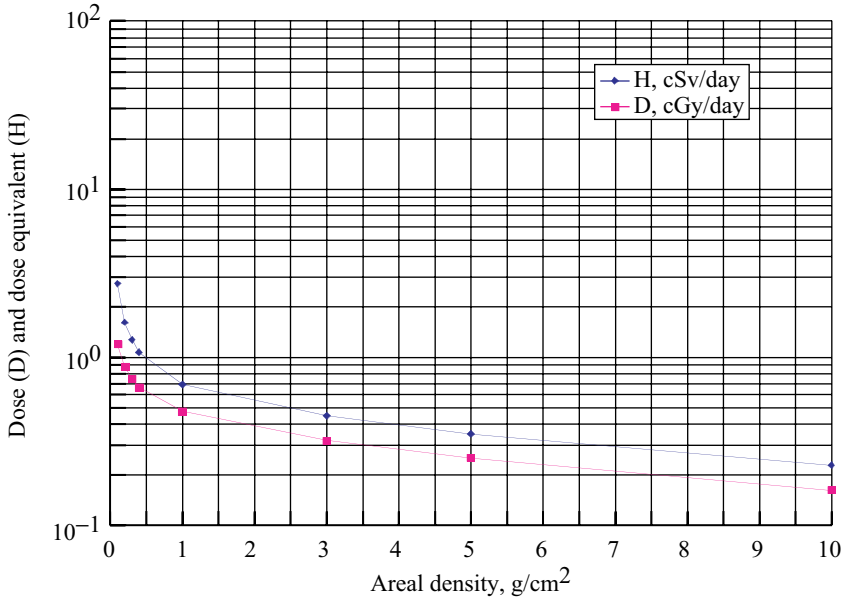

Figure 17. Dose versus depth in space suit fabric for STS-48 proton spectrum.

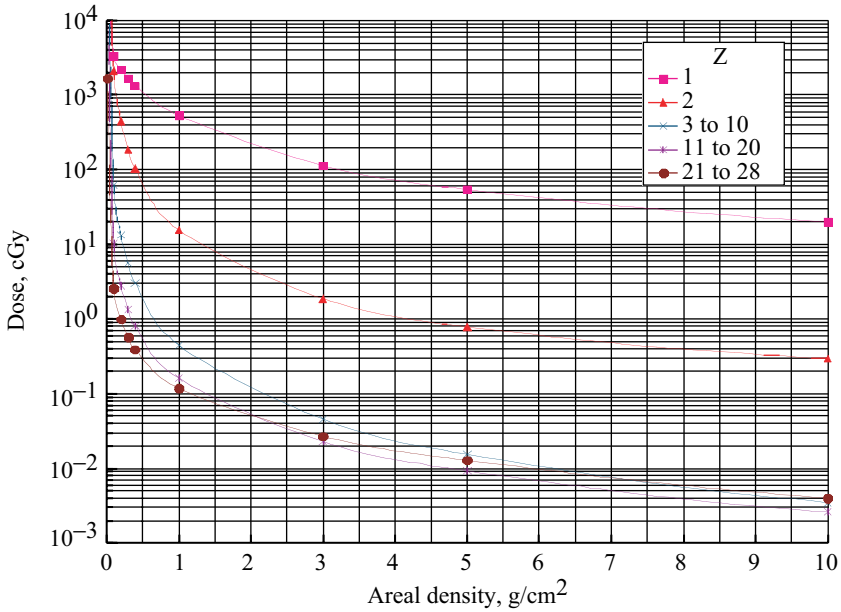

Figure 18. Dose versus depth in space suit fabric for September 29, 1989, SPE.

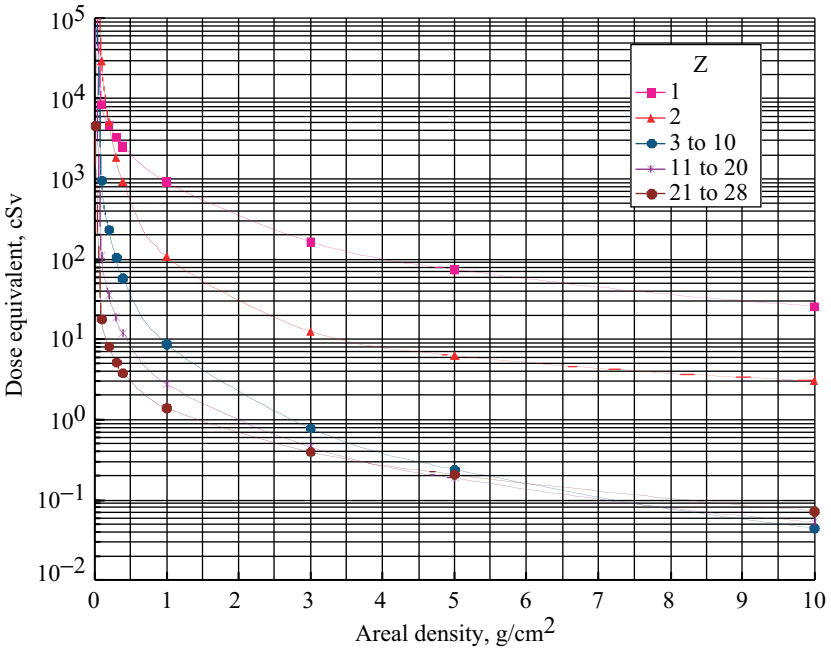

Figure 19. Dose equivalent versus depth in space suit fabric for September 29, 1989, SPE.

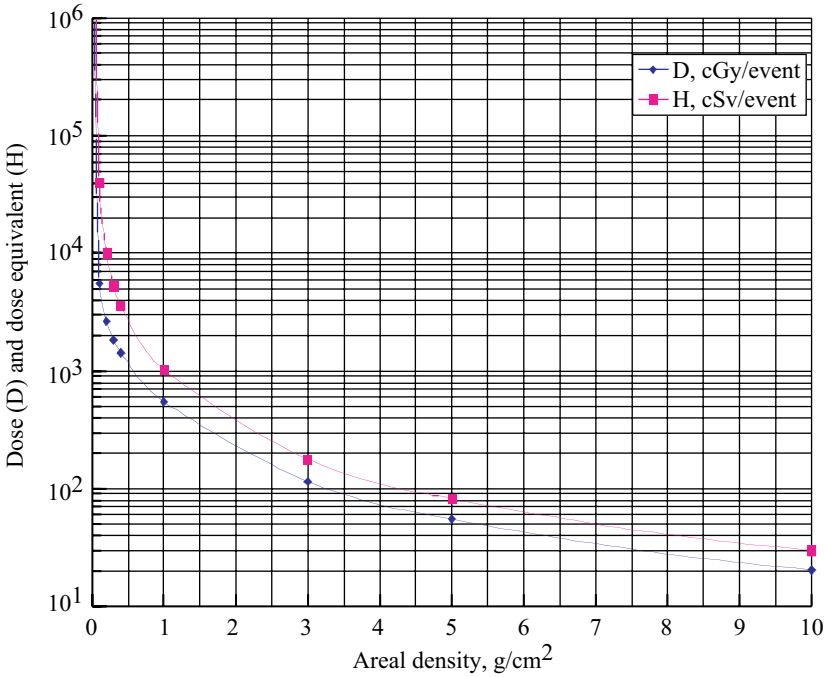

Figure 20. Total dose and dose equivalent in space suit fabric for September 29, 1989, SPE.

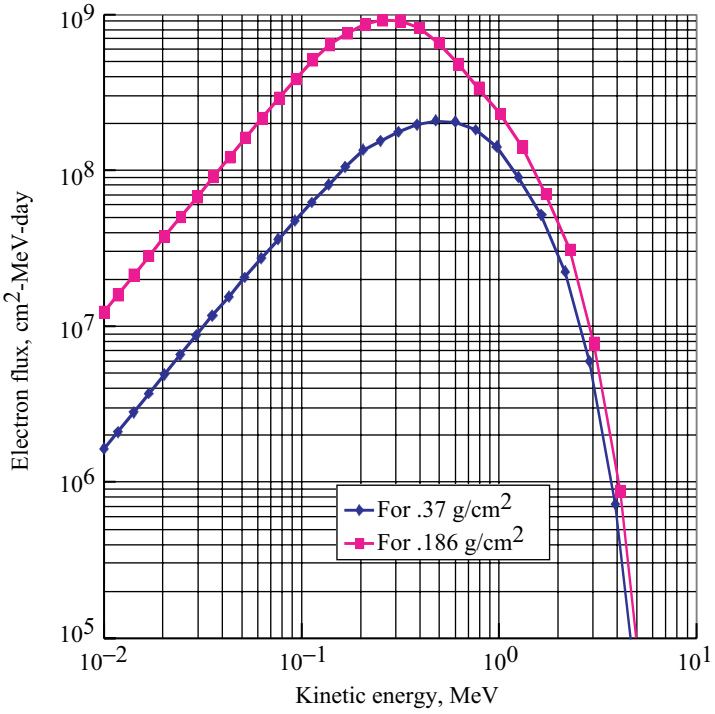

Figure 21. Sample spectra for LEO electrons in space suit fabric.

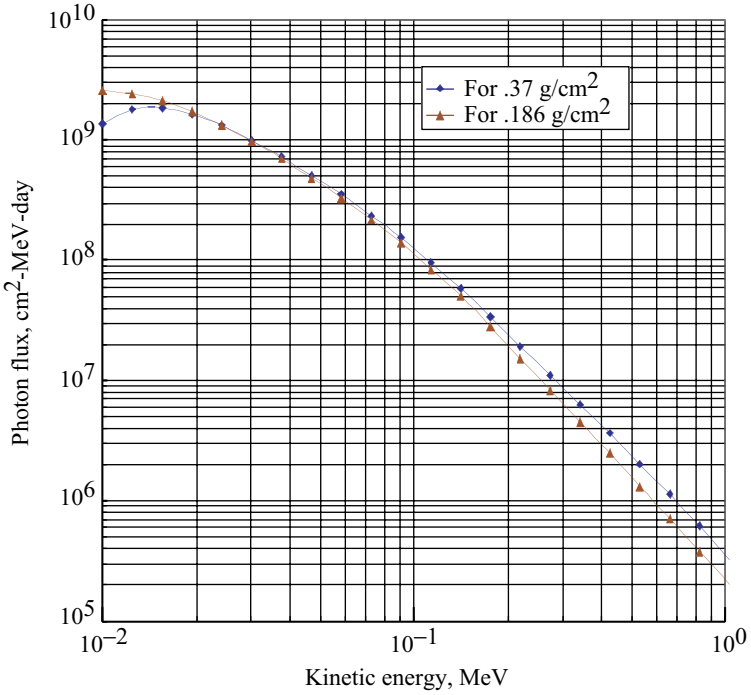

Figure 22. Sample spectra for LEO bremsstrahlung in space suit fabric.

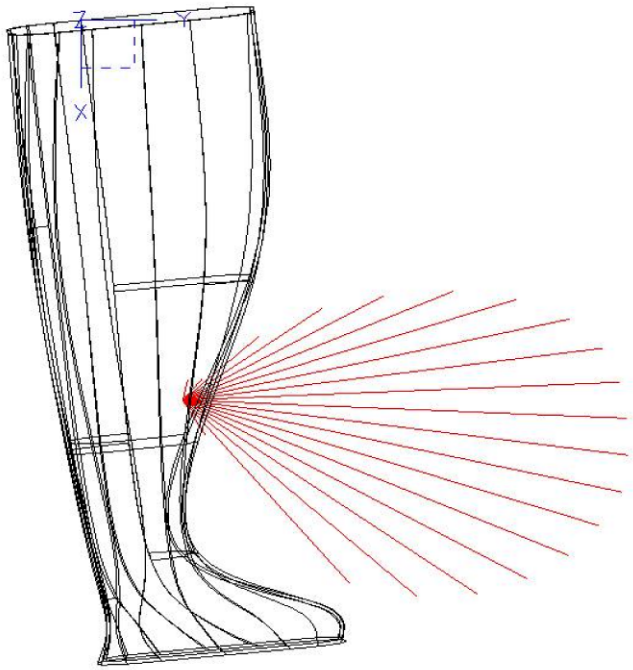

Figure 23. Directional dose variations for right shin target point.

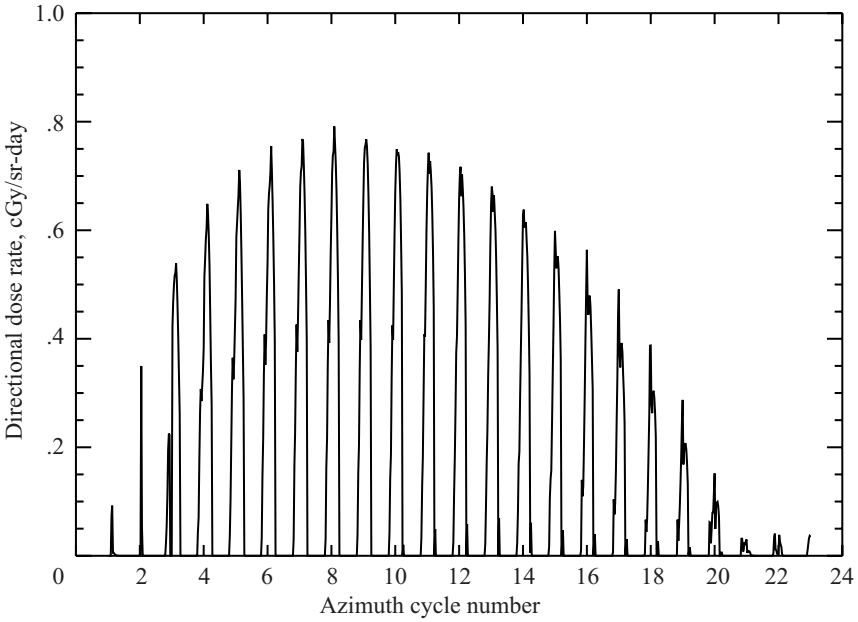

Figure 24. Directional dose values for right shin target point.

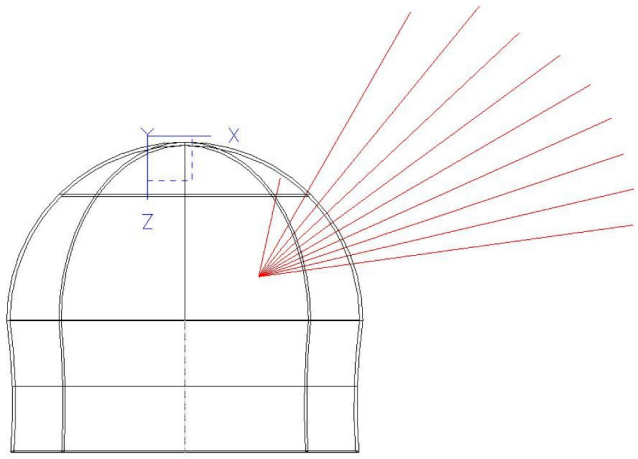

Figure 25. Directional dose variations of September 29, 1989, SPE on lunar surface for ocular lens.

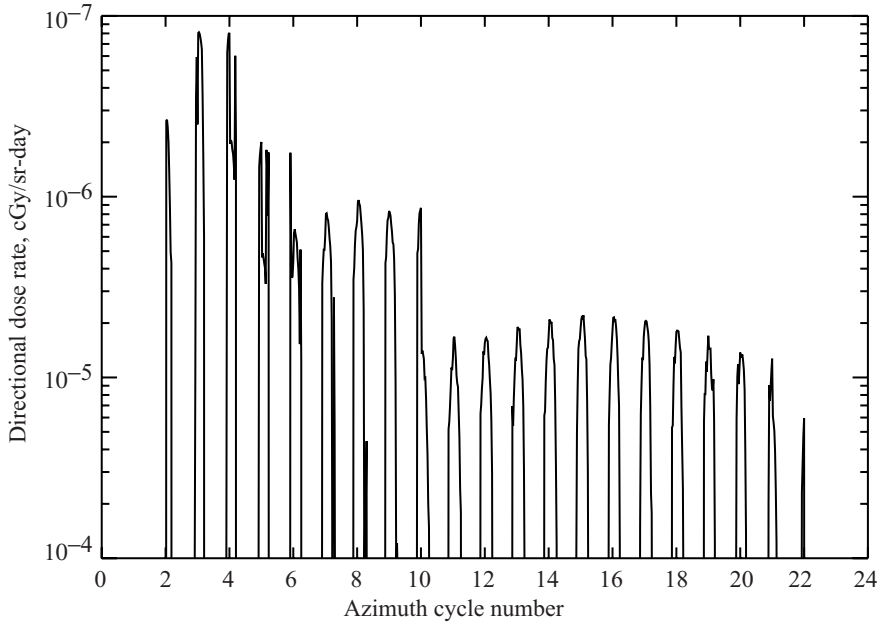

Figure 26. Directional dose values for right ocular lens.

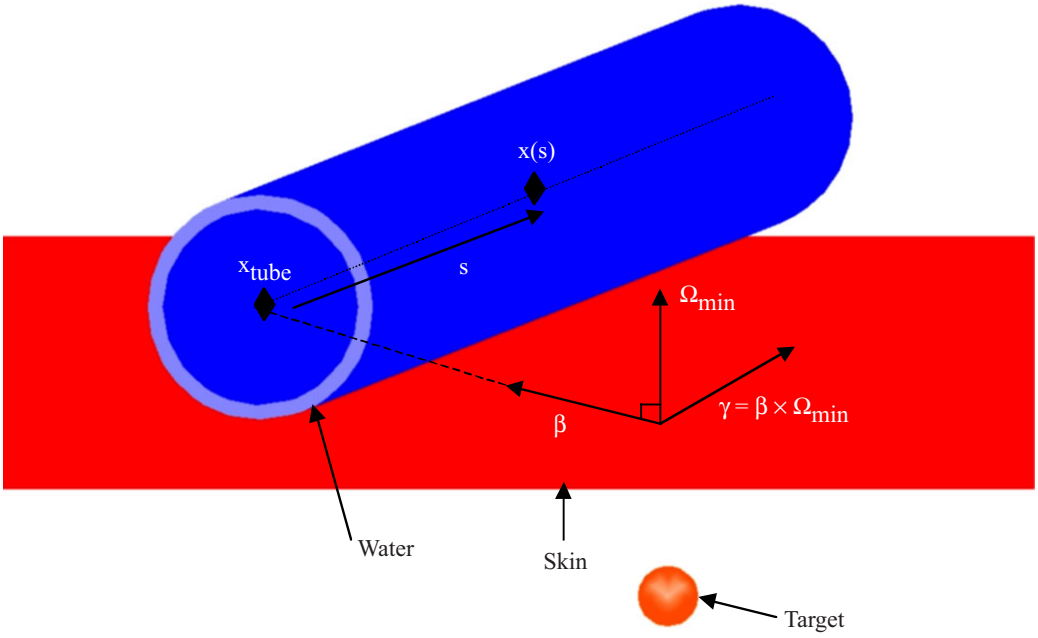

Figure 27. Display of coordinate system used to determine cord length.

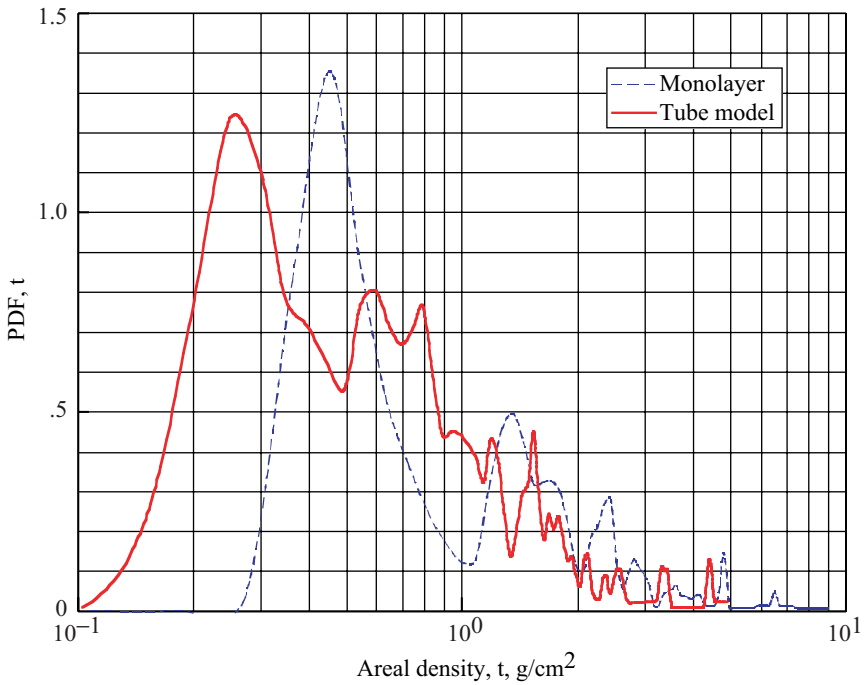

Figure 28. Probability density functions for thicknesses using monolayer and LCVG tube model calculations.

Appendix A

Description of CAD-Modeled Space Suit Components

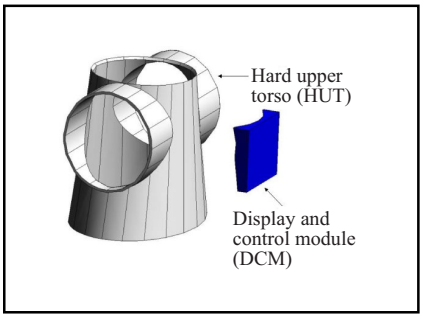

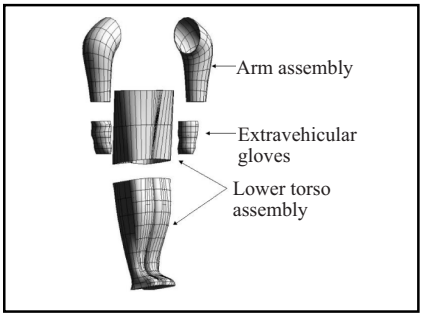

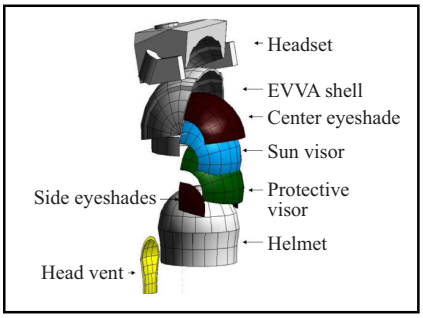

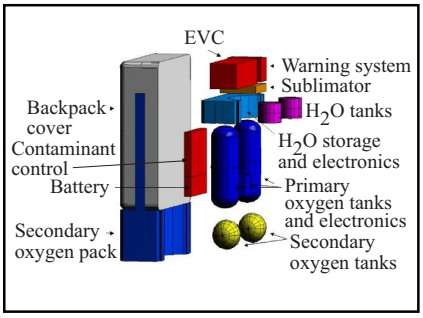

Component	Mass, kg	Model volume, cc	Computed density, g/cc	Composition (atom fraction)
HUT	3.52	2393	1.47	.18 H, .14 C, .02 N, .42 O, .04 F, l19 Si
DCM	5.52	2760	2.00	.27 H, .31 C, .16 O, .05 Si, l16 Fe, l05 Cu
Arm assembly	1.62	1857	0.872	.47 H, .37 C, .05 N, .11 O, .07 F, .003 Cl
EVA gloves	0.276	316	0.872	.47 H, .37 C, .05 N, .11 O, .07 F, .003 Cl
LTA	2.88	3300	0.872	.47 H, .37 C, .05 N, .11 O, .07 F, .003 Cl
Legs, ea.	1.43	1641	0.872	.47 H, .37 C, .05 N, .11 O, .07 F, .003 Cl
Headset	3.6	6984	0.515	.35 H, .41 C, .18 O, .053 Si
EVVA shell	1.49	1244	1.2	.42 H, .37 C, .09 O
Cen. eyeshade	0.66	364	1.8	.66 O, .33 Si
Sun visor	0.44	353	1.24	.41 H, .50 C, .07 O, .02 S
Prot. visor	0.43	366	1.2	.42 H, .37 C, .09 O
Helmet	0.61	505	1.2	.42 H, .37 C, .09 O
Side visors, ea.	0.065	35	1.8	.66 O, .33 Si
Head vent	0.12	99	1.2	.42 H, .37 C, .09 O
EVC	9.02	7800	1.16	.34 H, .39 C, .17 O, .05 Si, .05 Cu
Warning sys.	2.64	2280	1.16	.34 H, .39 C, .17 O, .05 Si, .05 Cu
Sublimator	1.6	1600	1	.67 H, .33 O
Water tanks, ea.	1.1	1099	1	.67 H, .33 O
Water S&C	8.35	7220	1.16	.27 H, .31 C, .16 O, .05 Si, .16 Fe, .05 Cu
Prim. O & Cont.	12.8	11002	1.16	.24 H, .28 C, .14 O, .04 Si, .22 Fe, .08 Cu
Sec. O tanks	1.29	1643	0.782	.19 Cr, .71 Fe, .10 Ni
Back cover	9.8	7568	1.29	.42 H, .37 C, .09 O
Contam. cont.	2.89	2760	1.05	.33 H, .33 Li, .33 O
Battery	4.48	1200	3.73	.33 O, .33 Zn, .33 Ag
Sec. O tanks	7.61	23416	0.325	.27 H, .31 C, .16 O, .05 Si, .16 Fe, .05 Cu

Appendix B

Nomenclature

C	chord length of ray traverse of cooling tube
D^2	distance squared from tube axis to dose point for arbitrary direction
p	probability density function for fabric thickness
r_0	cooling tube radius
s	distance from cooling tube to dose point
t	fabric thickness
t_b	body thickness
t_0	fabric mean thickness
x	arbitrary distance value
$\boldsymbol{x}$	arbitrary point on cooling tube axis
$\boldsymbol{x}_{\text{tube}}$	point on cooling tube axis nearest dose point
$\alpha_{1,2,3}$	direction cosines of unit vector $\boldsymbol{\Omega}_{\text{min}}$
$\beta_{1,2,3}$	direction cosines of unit vector $\boldsymbol{\beta}$
$\boldsymbol{\beta}$	unit vector specifying direction
$\boldsymbol{\gamma}$	unit vector parallel to local surface
θ	polar angle
κ	random number between 0 and 1
ν	magnitude of vector from dose point to tube axis
σ	mean deviation of fabric thickness
φ	azimuth angle
$\omega_{1,2}$	components of ray direction between $\boldsymbol{\beta}$ and $\boldsymbol{\Omega}_{\text{min}}$
$\boldsymbol{\Omega}_{\text{min}}$	unit vector normal to local surface

Subscripts:

i index (1,2,3)

im minimum value of variable α_i

m refers to fabric slant height thickness

min fabric thickness for normal incidence

ray refers to specific ray direction

Modeling of Suit Fabric and LCVG

In past analysis the suit's material and LCVG were modeled as a constant thickness with the tubes represented as a smeared mass throughout the suit. Testing of the suit fabric (described in table 2) with the LCVG (ref. 8) showed that this does not accurately represent the fabric and LCVG. The testing showed that due to the many layers of woven material throughout the fabric the thickness is variable. It also showed that the tubes provide a large amount of shielding for the skin underneath it while skin that did not have any tubes near it had much less shielding. Thus, additional modeling was required to more accurately represent the tubes.

In the modeling of the LCVG it is assumed that the spandex-nylon net is part of the suit's fabric while the ethyl-vinyl-acetate tubes filled with water lie on the surface of the skin, excluding the head, hands, and feet. In testing it was found that the suit's fabric, less the water-filled tubes, has a variable thickness of material (ref. 8) along a given path that is random according to

$$p(t) = \exp[-(t - t_0)^2/(2\sigma^2)]/(2\pi\sigma^2)^{1/2} \tag{B1}$$

where the mean thickness t_0 is 0.161 g/cm^2 (i.e., 0.280 g/cm^2 total thickness of the suit material minus that attributed to the tubes, 0.119 g/cm^2) and where σ is 0.03 g/cm^2. In the CAD model the fabric is of fixed thickness t_{min}, 0.280 g/cm^2, but rays passing through the surface in direction $\boldsymbol{\Omega}$ have thickness along the slant height $t_m(\boldsymbol{\Omega})$ and must be related to the fabric distribution of equation (B1). The ray thickness is then taken as a random variable in which

$$t_{ray}(\boldsymbol{\Omega}) = t(\kappa)\, t_m(\boldsymbol{\Omega})/t_{min} \tag{B2}$$

where κ is a uniform random number on the interval {0,1} and

$$t(\kappa) = t_0 + 2^{1/2}\, \sigma\, \mathrm{erf}^{-1}(2\kappa - 1) \tag{B3}$$

where erf^{-1} is the inverse error function and a different random number κ is taken for each ray direction. The scaling in equation (B2) represents the nonuniformity in the fabric observed in transmission testing (ref. 8).

The modeling of the water-filled tubes is likewise complicated in their representation within the CAD model. The tubes are located in parallel arrays separated by 1 cm (ref. 5). If it is assumed that the tubes are against the skin of the astronaut (represented by the CAM or CAF models) and the target point at

which the exposure is to be evaluated is random, then the problem is to find the probability that the rays passing through the dose point in fact passed through a section of the water-filled tube. Because the tubes are parallel and 1 cm apart, then for each target point only the two nearest tubes are considered. Because points remote from any tube (e.g., deep in the body) are little affected, only the skin target points are evaluated with the tubes.

The nearest tube to the target point lies near the ray of minimum distance to the surface of the skin. This ray direction $\boldsymbol{\Omega}_{\min}$ is found by searching over the body thickness function $t_b(\boldsymbol{\Omega})$ (given by the ray tracing) for the smallest value. At that point on the surface with minimum thickness to the dose point we place two tubes on opposite sides, one located at a distance $x(\kappa)$ given as

$$x(\kappa) = 0.5\kappa \text{ (cm)} \tag{B4}$$

where the second tube is at a distance $1 - x(\kappa)$ and κ is a uniformly distributed random number on the interval $\{0,1\}$ as before. However, whereas each direction $\boldsymbol{\Omega}$ has a separate κ in equation (B2), there is only one κ for each dose point in equation (B4). For a given $x(\kappa)$ and direction $\boldsymbol{\Omega}$ we require the chord through either of the two tubes. To calculate this chord, we require solving the appropriate geometry. The first is to define a coordinate system. Because $\boldsymbol{\Omega}_{\min}$ is assumed normal to the local surface, then any unit vector $\boldsymbol{\beta}$ such that $\boldsymbol{\beta}\cdot\boldsymbol{\Omega}_{\min} = 0$ is tangent to the local surface (e.g., the skin). We use an arbitrary tangent vector to define the direction to the tube and a unit vector $\boldsymbol{\gamma}$ parallel to the tube axis for the calculations. We take

$$\boldsymbol{\beta}\cdot\boldsymbol{\Omega}_{\min} = \beta_1\alpha_1 + \beta_2\alpha_2 + \beta_3\alpha_3 = 0 \tag{B5}$$

which we solve by finding $\alpha_{im} = \min\{\alpha_i\}$ and set $\boldsymbol{\beta}_{im} = 0$. The remaining $\boldsymbol{\beta}_i$ can be solved with the requirement of normalization to unity. The vector parallel to the tube is given as

$$\boldsymbol{\gamma} = \boldsymbol{\beta} \times \boldsymbol{\Omega}_{\min} \tag{B6}$$

The point on the tube axis located at $x(\kappa)$ along the surface nearest the dose point as defined above is

$$\boldsymbol{x}_{\text{tube}} = t(\boldsymbol{\Omega}_{\min})\,\boldsymbol{\Omega}_{\min} + x(\kappa)\boldsymbol{\beta} \tag{B7}$$

An arbitrary point on the tube axis is given as

$$\boldsymbol{x}(s) = \boldsymbol{x}_{\text{tube}} + s\,\boldsymbol{\gamma} \tag{B8}$$

where s is the distance along the tube measured from the point on the tube nearest the dose point. A visualization of these values is given in figure 27. We need the nearest point to the tube axis along an arbitrary direction $\boldsymbol{\Omega}$ to evaluate the chord for that ray. This is accomplished by finding the minimum of the distance D as

$$D^2 = \min_{s,\nu}\{[\boldsymbol{x}(s) - \nu\,\boldsymbol{\Omega}]^2\} \tag{B9}$$

The solution can be written as

$$D^2 = [t(\boldsymbol{\Omega}_{\min}) - \nu\,\omega_1]^2 + [x(\kappa) - \nu\,\omega_2]^2 \tag{B10}$$

where

$$\omega_1 = \boldsymbol{\Omega}_{\min} \cdot \boldsymbol{\Omega}$$

$$\omega_2 = \boldsymbol{\beta} \cdot \boldsymbol{\Omega}$$

are the components of ν along $\boldsymbol{\Omega}_{\min}$ and $\boldsymbol{\beta}$, respectively, where

$$\nu = [t(\boldsymbol{\Omega}_{\min})\omega_1 + x(\kappa)\omega_2] / \left[\omega_1^2 + \omega_2^2\right]^{1/2} \tag{B11}$$

The chord is, for D less than the tube radius r_0, given as

$$C = 2\left(r_0^2 - D^2\right)^{1/2} \tag{B12}$$

and has value zero for values of D greater than r_0. The material the ray must penetrate to reach the astronaut within the suit is the chord so that the total shielding is

$$t_{\text{ray}}(\boldsymbol{\Omega}) = t(\kappa) t_m(\boldsymbol{\Omega}) / t_{\min} + C \tag{B13}$$

Note that even if an intersection of the tube at $x(\kappa)$ is not found, the calculation is to be repeated by replacing $x(\kappa)$ with $x(\kappa) - 1$ for the second tube of the nearest pair. The chord of the next nearest pair is evaluated by replacing the $x(\kappa)$ by $x(\kappa) + 1$ and then by $x(\kappa) - 2$. The appropriate value(s) of C is (are) used (summed) in equation (B13).

In order to demonstrate the behavior of the orthofabric/tube calculation, a thickness distribution for the EMU was generated for the right shin target point vicinity (a region where attenuation is predominantly from the orthofabric and tube layers). The 968 thickness values along the rays about the target point were sorted into ascending order and used to construct cumulative distribution functions for both constant thickness and separate tube calculations. The corresponding probability density functions, PDF(t), were obtained by differentiation and are shown in figure 28.

The total dose, D, at the target point may then be found by integration:

$$D = \int \text{PDF}(t)\, D(t)\, dt$$

where $D(t)$ is the dose versus depth function (for this example, the curve for H_2O shown in fig. 28). The results give D = 9.92 cSv for the constant thickness calculation, and a value of D = 18.31 cSv with the detailed LCVG model invoked. (Note that no body shielding has been included in this calculation.)

REPORT DOCUMENTATION PAGE

Form Approved
OMB No. 0704-0188

1. REPORT DATE *(DD-MM-YYYY)*	2. REPORT TYPE	3. DATES COVERED *(From - To)*
01- 03 - 2003	Technical Publication	

4. TITLE AND SUBTITLE
Analysis of a Radiation Model of the Shuttle Space Suit

5a. CONTRACT NUMBER

5b. GRANT NUMBER

5c. PROGRAM ELEMENT NUMBER

6. AUTHOR(S)
Anderson, Brooke M.; Nealy, John E.; Kim, Myung-Hee; Qualls, Garry D.; and Wilson, John W.

5d. PROJECT NUMBER

5e. TASK NUMBER

5f. WORK UNIT NUMBER
732-50-00-01

7. PERFORMING ORGANIZATION NAME(S) AND ADDRESS(ES)
NASA Langley Research Center
Hampton, VA 23681-2199

8. PERFORMING ORGANIZATION REPORT NUMBER
L-18235

9. SPONSORING/MONITORING AGENCY NAME(S) AND ADDRESS(ES)
National Aeronautics and Space Administration
Washington, DC 20546-0001

10. SPONSOR/MONITOR'S ACRONYM(S)
NASA

11. SPONSOR/MONITOR'S REPORT NUMBER(S)
NASA/TP-2003-212158

12. DISTRIBUTION/AVAILABILITY STATEMENT
Unclassified - Unlimited
Subject Category 93
Availability: NASA CASI (301) 621-0390 Distribution: Standard

13. SUPPLEMENTARY NOTES
Anderson, Swales Aerospace. Nealy, Old Dominion University. Kim, College of William and Mary. Qualls and Wilson, Langley Research Center. (Anderson is now with Langley Research Center)
An electronic version can be found at http://techreports.larc.nasa.gov/ltrs/ or http://techreports.larc.nasa.gov/cgi-bin/NTRS

14. ABSTRACT

The extravehicular activity (EVA) required to assemble the International Space Station (ISS) will take approximately 1500 hours with 400 hours of EVA per year in operations and maintenance. With the Space Station at an inclination of 51.6° the radiation environment is highly variable with solar activity being of great concern. Thus, it is important to study the dose gradients about the body during an EVA to help determine the cancer risk associated with the different environments the ISS will encounter. In this paper we are concerned only with the trapped radiation (electrons and protons). Two different scenarios are looked at: the first is the quiet geomagnetic periods in low Earth orbit (LEO) and the second is during a large solar particle event in the deep space environment. This study includes a description of how the space suit's computer aided design (CAD) model was developed along with a description of the human model. Also included is a brief description of the transport codes used to determine the total integrated dose at several locations within the body. Finally, the results of the transport codes when applied to the space suit and human model and a brief description of the results are presented.

15. SUBJECT TERMS
Space radiation; Shuttle space suit

16. SECURITY CLASSIFICATION OF:			17. LIMITATION OF ABSTRACT	18. NUMBER OF PAGES	19a. NAME OF RESPONSIBLE PERSON
a. REPORT	b. ABSTRACT	c. THIS PAGE			STI Help Desk (email: help@sti.nasa.gov)
					19b. TELEPHONE NUMBER *(Include area code)*
U	U	U	UU	41	(301) 621-0390